Федеральное государственное автономное образовательное учреждение
высшего образования
«Московский физико-технический институт
(национальный исследовательский университет)»
Физтех-школа физики и исследований им. Ландау
Физтех-кластер академической и научной карьеры (Квантовые наноструктуры, материалы и устройства)

Направление подготовки / специальность: 03.04.01 Прикладные математика и физика
Направленность (профиль) подготовки: Общая и прикладная физика

ИЗГОТОВЛЕНИЕ И ИССЛЕДОВАНИЕ ПЛАНАРНОГО ДЖОЗЕФСОНОВСКОГО ПЕРЕХОДА НА ОСНОВЕ NB И AL

(магистерская диссертация)

Студент:
Полевой Константин Борисович

_____
(подпись студента)

Научный руководитель:
Столяров Василий Сергеевич,
канд. физ.-мат. наук

_____
(подпись научного руководителя)

Консультант *(при наличии)*:
_____
_____
(подпись консультанта)

Москва 2022

Skoltech

Skolkovo Institute of Science and Technology

MASTER'S THESIS

Fabrication and research on planar Josephson junction based on Nb and Al

Master's Educational Program: Center for Energy Science and Technology

Student_____

Konstantin Polevoy

Center for Energy Science and Technology

June, 2022

Research Advisor:_____

Albert Nasibulin

Professor

Co-Advisor:_____

Vasily Stolyarov

PhD

Moscow 2022

Skolkovo Institute of Science and Technology

МАГИСТЕРСКАЯ ДИССЕРТАЦИЯ

Изготовление и исследование планарного джозефсоновского перехода на основе Nb и Al

Магистерская образовательная программа: Центр фотоники и квантовых материалов

Студент_____

Константин Полевой

Центр фотоники и квантовых материалов

Июнь, 2022

Научный руководитель:_____

Альберт Насибулин

Профессор

Со-руководитель:_____

Василий Столяров

к.ф.-м.н.

Москва 2022

Fabrication and research on planar Josephson junction based on Nb and Al

Konstantin Polevoy

Submitted to the Skolkovo Institute of Science and Technology
on June, 2022

Abstract

Ultra-low dissipating digital superconducting computing is a promising alternative to conventional semiconductor computers. The Josephson junction is the key element of the new kind of electronics. Typically, such devices use tunnel junctions based on insulating barrier. But they should be shunting, in order to avoid hysteresis behaviour. This approach wastes a lot of space due to large size of each elements of circuits. As an alternative, a planar Josephson junction in a variable- thickness bridge geometry has been proposed. In our days, it is inferior to the tunnel junction in terms of characteristic stresses. But recently a planar Josephson junction with linear dimensions smaller than the coherent length has been proposed. It was predicted that such a weak ling should have high characteristic voltages and be free of hysteresis.

This work presents the process of realization of such a Josephson junction and the results of measurements of current-voltage characteristics in a wide temperature range. Variable thickness bridges showed high characteristic voltage of the order of $1\ mV$, which greatly exceeded the characteristic stresses of the used tunnel contacts. The achievement of critical current densities up to $40\ mA/\mu m^2$ was also demonstrated, which was accompanied by the absence hysteresis up to 10 mK on all measured samples.

Research Advisor:
Name: Albert Nasibulin
Degree:
Title: Professor

Co-Advisor:
Name: Vasily Stolyarov
Degree:
Title: PhD

Изготовление и исследование планарного джозефсоновского перехода на основе Nb и Al

Константин Полевой

Представлено в Сколковский институт науки и технологий
Июнь, 2022

Реферат

Цифровые сверхпроводящие вычисления со сверхнизким рассеиванием энергии являются многообещающей альтернативой обычным полупроводниковым компьютерам. Переход Джозефсона — ключевой элемент электроники нового типа. Обычно в таких устройствах используются туннельные переходы на основе изолирующего барьера. Но такие барьеры должны быть шунтироваться, чтобы избежать гистерезисного вида вольт-амперных характеристик. Этот подход занимает много места из-за большого размера каждого элемента схемы. В качестве альтернативы был предложен планарный джозефсоновский переход в геометрии моста переменной толщины. В наши дни он уступает туннельному узлу по характерным напряжениям. Но недавно был предложен планарный джозефсоновский переход с линейными размерами меньше когерентной длины. Было предсказано, что такая слабая линия должна иметь высокие характеристические напряжения и не иметь гистерезиса.

В данной работе представлен процесс реализации такого Джозефсоновского перехода и результаты измерений вольтамперных характеристик в широком диапазоне температур. Мостики переменной толщины показали высокие характеристические напряжения порядка 1 мВ что сильно превышает характеристические напряжения используемых туннельных контактов. Так же продемонстрировано достижение плотностей критического тока вплоть до 40 мА/мкм^2, что сопровождалось отсутствием гистерезиса вплоть до 10 мК температур на всех измеренных образцах

Научный руководитель:
Имя: Альберт Насибулин
Ученое звание, степень:
Должность: Профессор

Со-руководитель:
Имя: Василий Столяров
Ученое звание, степень:
Должность: к.ф.-м.н.

Acknowledgments

First of all, I would like to thank the scientific advisor, Vasily Stolyarov, for the opportunity to work and get results in the TQPSS laboratory. I hope this is a serious start for further scientific career.

I was glad to work at TQPSS lab with each of members.

Also, I would like to thank Andrey Shishkin for the hours spent in the clean room together and for help with the samples fabrication. I also express my deep gratitude to Sergey Egorov for the help at the final stage of sample fabrication.

Special thanks to the Head of Quantum Nanostructures, Materials and Devices Prof. Valery Ryazanov and Prof. Galina Tsirlina for providing educational background.

And many thanks to Professor Albert Nasibulin for his supervision in Skoltech, comments and openness to students.

Contents

List of Figures

Chapter 1

Introduction

Digital epoch started in the previous centre with width a wide spread of semiconductor computers. While efficiency of micro-scheme had enormous jump, during all the history approaching near limit was predicted at each time period. That's why computers with distinguished principles of work always were paid much attention.

One of the parallel research was related to application of superconductors. In 1962 weakling was investigated[3]. Lately, it was suggested as an key element for superconducting computers. Through the several implementations and transformations, current stable version based on Nb and AlOx combination became actively used. While such approach don't show supremacy, it is still promising direction for researcher. Stable approach in our days, is RSFQ logic[4]. As a Josephson junction tunnel barrier with required shunting resistor is commonly used. And it is one of limitation to density of elements. Some restrictions can be removed in case of application of so-called self-shunting weak-links. Such approach will help to save area on the order by 11.1. While high critical

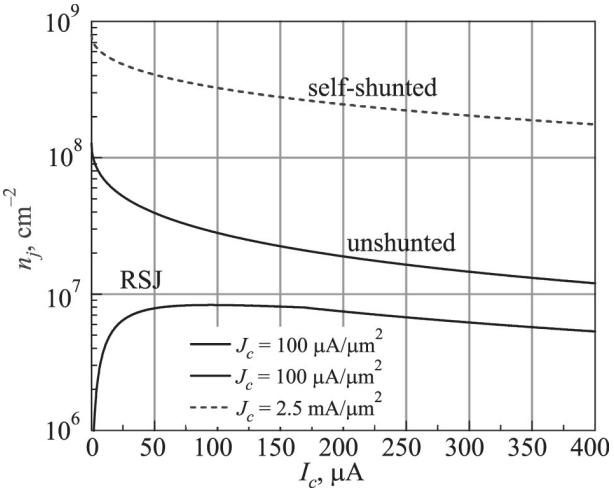

Figure 1.1: Limitations on the density of elements in RSFQ logic, in cases of different Josephson junctions. Picture form article [1]

current densities often go together with self-shunting, geometry of planar JJ with sizes less then superconducting coherent length ξ_N was suggested. At this work fabrication of such weak link described.

In the section **Background** introduced basic knowledge about superconductivity, and Josephson junctions. Also short history of superconducting computing is discussed. Finally, weak-link

in the geometry of Variable-Thickness bridge(VTB) is described.

In the section **Equipment** methods and equipment, which used during the work, are described.

In the section **Results and Discussion** results of measurements are shown.

Chapter 2

Background

2.1 Superconductivity

Superconductivity is a macroscopic quantum phenomena. The main properties are zero resistance under DC current and magnetic field pushing out of bulk material. Two types of superconductors are distinguished.

Type-I superconductors under external magnetic field have superconducting currents on the edges, which suppress magnetic field deep into bulk material. Higher fields have larger penetration length. At some critical field superconducting currents can't screen the field and superconductivity disappear.

Type-II superconductors have two critical fields H_{1c} and H_{c2}. In fields less than H_{1c} behavior is similar to Type-I superconductor. Between critical fields Abrikosov vortexes are formed. And in field above H_{c2} superconductivity is fully suppressed.

2.2 Bardeen–Cooper–Schrieffer theory

In the Bardeen-Cooper-Schrieffer theory, the existence of superconductivity is explained by the **attracting** interaction of electrons via phonons.[2] That interaction leads to the formation of an energetically more favorable state, when electrons are densely packed near the Fermi surface. Due to the fact that on the boundary of the Fermi surface there are available electron states of electrons, electron scattering becomes possible in a spherical layer with a thickness of the order of $\overline{h}\omega_D$. So, small loss in kinetic energy leads to a larger gain in interaction energy. Here ω_D is the Debye frequency.

For pair scattering to become possible, two conditions must be satisfied: the states from which scattering occurs must be occupied, and the states into which scattering occurs must be free. Therefore, electrons are combined into pairs with equal in magnitude and opposite in direction momenta and spins. The excitation over the new ground state is considered to be a single electron. Excitation spectrum calculated in the BCS theory:

$$E_k = \sqrt{\epsilon_k^2 + \Delta^2(T)} \tag{2.1}$$

where $\epsilon_k = \frac{\hbar k^2}{2m} - \frac{\hbar k_F^2}{2m}$ is kinetic energy of electrons over Fermi level. It's clear excitations have energy above $\Delta(T)$. That's why the energy is required to destroy Cooper's pair is $2\Delta(T)$.

Connection between energy gap and superconductivity can be explained as follows. At low temperatures scattering on defects has the main contribution to resistivity. For superconductor, scattering of Cooper pair means formation of two electron excitation with energies Δ. Small currents don't enough to provide such energy, so scattering don't happens.

2.3 Ginzburg–Landau theory

The superconducting state is more ordered than the normal state. The transition between them is a phase transition of the second order. So there must be some order parameter. The wave function $\psi(r)$ of superconducting electrons was chosen, and $|\Psi|^2 = \frac{n_s}{2}$, where n_s is the density of superconducting electrons, the square modulus of the wave function $|\Psi|^2$ is equal to the density of Cooper pairs. Then the expansion of the free energy density of the superconductor near T_c will have the form[2]:

$$G_s = G_n + \alpha|\Psi|^2 + \frac{\beta}{2}|\Psi|^4 + \frac{1}{4m_e}| - i\hbar\nabla\Psi - \frac{2e}{c}\vec{A}\Psi|^2 + \frac{H^2}{8\pi} - \frac{\vec{H}\cdot\vec{H}_0}{4\pi} \tag{2.2}$$

G_n is responsible for the free energy density in the normal state, the gradient term is responsible for the kinetic energy of superconducting electrons, H^2 term is responsible for the magnetic energy density. $\vec{H}_0$ is the the external uniform magnetic field. Minimization of the total free energy by the method of variation in Ψ^* and $\vec{A}$ yields the first and second Ginzburg-Landau equations:

$$\alpha\Psi + \beta\Psi|\Psi|^2 + \frac{1}{4m}\left(i\hbar\nabla + \frac{2e}{c}\vec{A}\right)^2\Psi = 0 \tag{2.3}$$

$$\vec{j_s} = -\frac{i\hbar e}{2m}\left(\Psi^*\nabla\Psi - \Psi\nabla\Psi^*\right) - \ frac2e^2mc|\Psi|^2\vec{A} \tag{2.4}$$

After substituting $\Psi_0^2 = n_s/2 = |\alpha|/\beta$, $\psi(r) = \Psi(r)/\Psi_0$, $\xi^2 = \frac{\hbar^2}{4m|\alpha|}$, $\lambda^2 = \frac{mc^2}{4\pi n_s e^2}$ the equations will take the form:

$$\xi^2\left(i\nabla + \frac{2\pi}{\Phi_0}\vec{A}\right)^2\psi - \psi + \psi|\psi|^2 = 0 \tag{2.5}$$

$$rot\, rot\vec{A} = -i\frac{\Phi_0}{4\pi\lambda^2}\left(\psi^*\nabla\psi - \psi\nabla\psi^*\right) - \frac{|\psi|^2}{\lambda^2}\vec{A} \tag{2.6}$$

ξ is the coherence length, the characteristic scale on which the wave function changes, λ is the penetration depth of a weak magnetic field into a superconductor.

2.4 Proximity effect

In the case of contact of a superconductor with a normal metal, Cooper pairs can penetrate through the boundary between them . This leads to a decrease of the order parameter in superconductor near the boundary on the scale of order ξ. In a normal metal, the order parameter decreases at distances of the order of , the decay length ξ_N. This parameter can be calculated from microscopic theory when the mean free path of electrons is $l_n \gg \xi_n$ (clean limit) and $l_n \ll \xi_n$ (dirty limit).

$$\xi_N = \frac{\overline{h} v_F}{2\pi k_B T} \, , l_n \gg \xi_N \tag{2.7}$$

$$\xi_N = \sqrt{\frac{\overline{h} D_n}{2\pi k_B T}} \, , l_n \ll \xi_N \tag{2.8}$$

where $D_n = \frac{v_F l_n}{3}$ is the diffusion coefficient in the metal. Suppression parameter $\gamma = \frac{\rho_s \xi_s}{\rho_n \xi_n}$

2.5 Josephson effect

The phenomenon of weak superconductivity was predicted by Josephson in 1962 [3] for a system of two superconductors separated by an insulator. Later, junctions where superconductivity is suppressed in one of the ways, insulator, a normal metal, a constriction of a superconductor, etc., began to be called Josephson junctions, or weak link. (Therm "weak link" usually used to distinguish structures with direct conductivity from tunnel junctions[5]) The non-dissipative current flowing through the weak-link depends on the phase difference ϕ of the wave functions of the superconducting electrons from different sides and is determined by current-phase relation $I\,(\phi))$ [6]. Its properties include $2\pi - periodicity$, existing of maximum current and zero current at zero phase difference. The maximum current through the Josephson junction $I_c(\phi)$ is called critical. For the first time, such a dependence was given for the superconductor-insulator-superconductor (SIS-contact) transition.

$$I_s(\phi) = I_c \sin\phi \tag{2.9}$$

But this relation isn't universal. For example, in the case of SNS in clean limit and very low temperatures has a sawtoothed form[7]:

$$I_s(\phi) = I_c(\phi/\pi), \; -\pi < \phi < \pi \tag{2.10}$$

At temperatures close to critical temperature current-phase relation also obeys to equation2.9, in other words, in the case when Giznburg-Landau theory can be applied.

If current though the junction exceed I_c, voltage on the JJ appears. Phase difference on the JJ obeys equation2.11:

$$2eV = \overline{h}\frac{\partial\phi}{\partial t} \tag{2.11}$$

and whole current thought the junction consist of superconducting and normal parts. In the case of current-phase relation for SIS 2.9 we will get:

$$I = I_c \sin\phi + \frac{\overline{h}}{2eR_n}\frac{\partial\phi}{\partial t} \tag{2.12}$$

where R_n is a normal resistance of JJ. In this case voltage is time-dependant and changes periodically:

$$V(t) = R_n\frac{I^2 - I_c^2}{I + I_c\cos\omega t} \tag{2.13}$$

where $\omega = \frac{2e}{\overline{h}}R_n\sqrt{I^2 - I_c^2}$. And average voltage has a form:

$$2e\overline{V} = \overline{h}\omega \tag{2.14}$$

2.6 Resistively Shunted Junction

For tunnel SIS junctions the resistively-shunted model (RCSJ) can be applied [8]. A Josephson junction is represented as a parallel connection of an ideal Josephson junction, a resistor, and a capacitance. This model describe behaviour of Josephson junction when currents are above critical currents. The normalized equation for the dependence of the current through such a contact on the phase difference ϕ has the form:

$$I/I_c = \beta_C\omega_c^{-2}\ddot{\phi} + \omega_c^{-1}\dot{\phi} + \sin\phi \tag{2.15}$$

where I_c is the Josephson junction critical current, $\omega_c = \frac{2e}{\overline{h}}I_cR$ is the Josephson frequency, $\beta_C = \frac{2e}{\overline{h}}I_cCR^2$ - McCumber parameter. The first term on the right side is responsible for the bias current in the capacitor, the second term for the current through the resistor, and the last term for the current through an ideal Josephson junction with a sinusoidal current-phase relationship. The return current (the current at which the voltage becomes zero again) depends on the β_C parameter. Decrease of β_C leads to approach of the return current is to the critical one, and hysteresis becomes smaller. (Fig. 2.1)

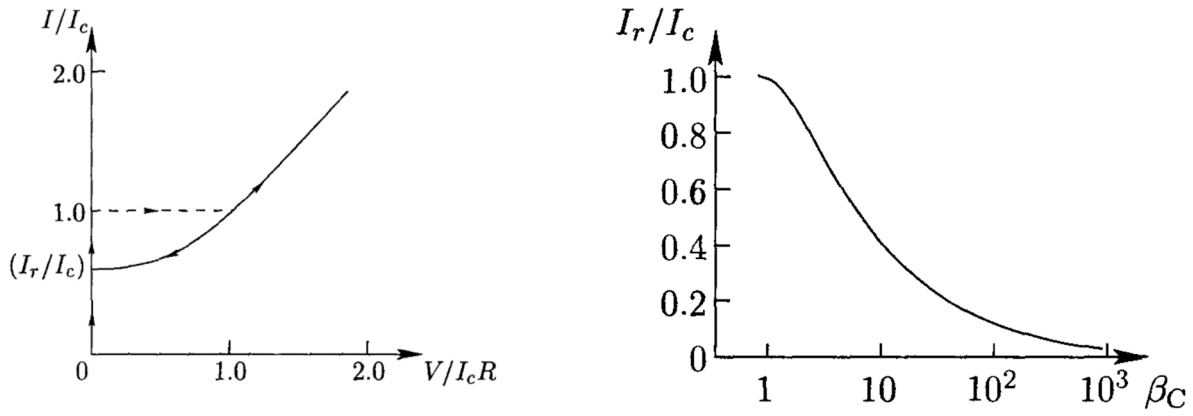

Figure 2.1: Voltage characteristic and dependence of return current on McCumber parameter [2]

2.7 Hysteresis in SNS

While in SIS junctions hysteresis can be described using RCSJ model, SNS junctions have incomparably less capacitance, so we should expect absence of hysteresis at proximity junctions. But it isn't true. In SNS junctions at very low temperatures difference between critical current I_c and retrapping current I_r observed. The same effect can be observed in point-contact weak link[9], nanowires[10], normal metals[11]. All over the time two main explanations were suggested. The first one is overheating due to Joule power[9]. That means what on backward curve temperature of contact locally higher then temperate of environment, that's why critical current reduced. Second approach suggests that response time R_nC should be replaced by a time $\overline{h}/\Delta$ related to the superconducting gap Δ [12] or by the electron diffusion time L^2/D through the junction [11]. But in the most recent research [13] it has been shown, that hysteresis in such systems related with the fact, that electron temperature in JJ is higher then temperature of environment. It occurs due to bad heat exchange between electron and phonon subsystems at low temperatures, because of small number of phonons. At higher temperatures hysteresis disappear while temperatures of electron and phonon subsystems become equal.

2.8 Superconducting electronics

While superconductors almost faced physical limit of operation frequencies at the point of several GHz, only ways to increase efficiency of current computers is increasing number of cores and threads, and programs improving and adapting to parallel performance. At the same time superconductors have a large potential in realization of superconducting electronics. Physical limits for clock frequencies on the order of hundreds of GHz. That is why this research direction still under development, despite the fact semiconductor technology has been remaining more efficient during last decades.

Usually, when listing advantages of superconducting electronics over semiconductor electronics, the next topics are mentioned: extremely fast switching and low power dissipation. Low operation temperature can be considered as disadvantage, while it requires complicated cooling equipment, but at the same time thermal noise less then for semiconductors. In our days one of the promising approaches for superconducting computers is RSFQ-logic.

2.8.1 Previous achievements

One of the latest previous approaches was superconducting circuits by IBM group at the beginning of 1980's[14]. They used combination of Pb alloys (specifically Pb with Au and In) as superconductor and Nb-oxide as an insulator for JJ. JJ was under-dumped, in other words with hysteresis and so-called latching logic. For "0" JJ the state with $V = 0$ was responsible, and for "1" the state with $V \neq 0$. Current trough the JJ consisted of bias current I_b close to critical current I_c and arriving signal I_{in}, which adds to bias current and together they can exceed critical current and switch JJ from state "0" to "1". Because of hysteresis, without I_{in} JJ remained at "1" state. In order to reset bit to initial "0" state, I_b should be turned off. It was done with external RF power supply.

Combination of Pb-alloy and Nb-oxide had one serious problem. Several circles of cooling and heating between $4\ K$ and $300\ K$ led to degradation of JJ. In the middle of 1980's this problem was resolved by replacing wit more robust combination of Nb as a superconductor and Al-oxide as a tunnel barrier. This materials still widely used in our days. Even such improvement didn't increase operation frequencies upper several GHz. But in 1980's it was great achievement compare with semiconductor computers. It was because of chosen latching logic Apparent problems for this approach were: supposed presence of external RF power supply, which means presence of external global timing for the circuit and supply. As a result, maximum operating frequencies are limited by external clocking. Next, RF supply should produce current to provide **all** JJ, so whole current supposed to be on order of 100 mA. Also, every JJ at resistive state constantly produced heat. Introduced Single-Flux-Quantum (SFQ) logic free from that issues[4].

For this logic over-dumped Josephson junction are used. The key idea is to use superconducting loop with JJ as a storage of information. Trapped magnetic flux decodes information. Applied current pulse to JJ, which turns JJ to resistive state for a short time period, allow to move magnetic flux to the neighboring loop. While the weak link don't has a hysteresis, when pulse ended, junction goes back to superconducting state. Rapid-Single-Flux-Quantum is a modification on SFQ, where JJ interconnected with another JJ. Also, one of the varieties of the basic cells of RSFQ logic is a superconducting ring with a Josephson junction with a ferromagnetic weak coupling included in it, $\pi - contact$. The 2π-periodicity of the current-phase characteristics makes it possible to change the direction of the superconducting current through the ring, passing between

the conditional states ”0” and ”1”, on which one can build various computational operations[4]. The advantages achieved today are high clock frequencies up to 100 GHz [1], which is an order of magnitude higher than the maximum possible 4 GHz for semiconductor microelectronics, and low heat dissipation per switch.

Important characteristic for JJ in superconducting circuits is characteristic voltage $V_c = I_c R_n$. Pulse time to switch JJ is proportional to V_c [4]. To achieve high V_c tunnel JJ are used. But they have hysteresis. So, JJ usually shunted with parallel resistor, to obtain a McCumber parameter of order 1 and make JJ overdumped . But this approach greatly increases the size of the base cell, which ultimately limits the density of the elements. [1] notes that the maximum density of shunted Josephson junctions in SFQ5ee technology at a critical current density $J_s = 100\ \mu A/\mu m^2$ is about $10^7 cm^{-2}$, which is three orders of magnitude less than the density of modern CMOS transistors.

One of the possible ways out of this situation can be the use of Josephson junctions with self-shunting. As noted in [15], [16], for the widely used Nb/Al combination, when sufficiently high values of the critical current density are reached, the hysteresis either greatly decreases or disappears altogether. Such an approach would increase the maximum degree of integration by several orders of magnitude. An estimate from [1] gives the contact density order of $10^9\ cm^{-2}$ for critical current densities $J_s = 2.5\ mA/\mu m^2$

2.9 Usadel equations

Usadel equation can be obtained from Eilenberg equations at dirty limit with using of functions F and G, dependant only on coordinate and ”Matsubara frequencies” [5]

$$2\overline{h}\omega_n F_n - \overline{h}D\left(\nabla - i\frac{2e}{\overline{h}c}\vec{A}\right)\left(G_n\left(\nabla - i\frac{2e}{\overline{h}c}\vec{A}\right)F_n - F_n\nabla G_n\right) = 2G_n\Delta \tag{2.16}$$

Where $G_n = \sqrt{1 - F_n\overline{F}_n}$, ”Matsubara frequency” $\overline{h}\omega_n = \pi kT\,(2n+1)$. Order parameter $\Delta(r)$ and super-current $j_s(r)$ are determined by relations:

$$\Delta \ln\frac{T_C}{T} = 2\pi kT\sum_{\omega>0}\left(\frac{\Delta}{\overline{h}\omega_n} - F_n\right) \tag{2.17}$$

$$\vec{j_s} = \frac{2\pi kT\sigma_N}{e} Im\sum_{\omega>0}\left(\overline{F}_n\left(\nabla - i\frac{2e}{\overline{h}c}\vec{A}\right)F_n\right) \tag{2.18}$$

Usadel equations can be simplified introducing function $\Phi_n(r)$:

$$F_n = \frac{\Phi_n}{\sqrt{(\overline{h}\omega_n)^2 + \Phi_n\overline{\Phi}_n}},\ G_n = \frac{\overline{h}\omega_n}{\sqrt{(\overline{h}\omega_n)^2 + \Phi_n\overline{\Phi}_n}} \tag{2.19}$$

After substitution, in case of $\vec{A} = 0$ we can obtain:

$$2\Phi_n G_n - \frac{\overline{h}D}{\overline{h}\omega_n}\nabla\left(G_n^2\nabla\Phi_n\right) = 2G_n\Delta \tag{2.20}$$

2.10 Variable thickens bridge

Geometry of planar JJ or more correctly variable-thickness bridge (VTB) were proposed two aciewe high critical current densities[17]. This geometry isn't new and there are a lot of papers devoted to VTB. Due to not so developed production technology most of them in the long dirty limit of SNS junctions, and most of works about JJ based on materials differed from combination of Nb and Al. Long submicron SNS based on Al and Nb described in [18]. At this case it was produced with deposition through mask and etching, Obtained length was 250 nm with width 1000 nm. Authors emphasised low characteristic voltage$V_c = 50\mu V$, which was related with unclear interfaces. Also long JJ based on Nb/Al/Nb produced by shadow evaporation was described and measured in work [19]. Based on V and Cu planar SNS produced with shadow evaporation with critical temperature 2.5K was reported in the work [20]. Described JJ had a length upper 420 nm. While the critical temperature was $T_c = 5.4\ K$, superconductivity disappeared at temperature above $T = 2.5\ K$. Meanwhile some of the samples were hysteresis free and for other samples hysteresis disappeared at temperatures above 1K. This was still not enough to operate at standard $4\ K$ refrigerators, but in principal it can be used in devices. Planar weak link with intermediate length from 65 nm to 230 nm was reported in the work [21]. It was based on Al and Cu combination, where ξ_N was on the order length of bridge. Also Shadow evaporation technique was used. For Al critical temperature $T_c = 1.2K$ junctions showed hysteresis at temperatures below $T = 0.6\ K$. Also Nb/Cu/Nb and Nb/NbOx/Nb short VTB with 100 nm length were reported in [22]. Work don't show the experiment and just concentrated on technology of evaporation trough the stable mask Au/PMMA or Al/PI.

As can be seen previous works were about nor materials different from Nb/Al combination, nor about long range. And most of them had shown hysteresis, and they had superconducting state at temperatures below 4 Kelvins. Motivation for works about stable masks is to achieve high rate of successful samples. For Nb and Al combination it is very important, because of very high temperature during evaporation during electron beam evaporation.

2.11 Usadel equation in case of planar SNS

In order to achieve high critical current densities, planar SNS with deep sub-micron sizes was proposed [17] (Fig 2.2). The small thickness of the normal layer and the width of the bridge, compared

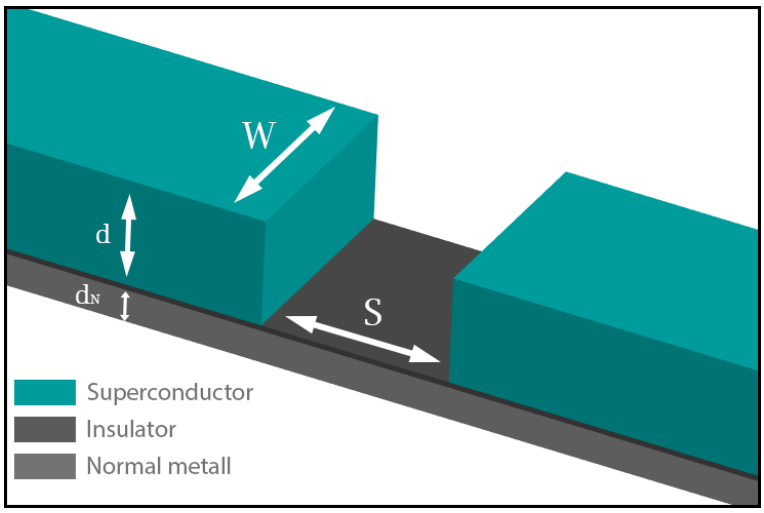

Figure 2.2: Schematic representation of the calculated structure.

to the coherence length in a normal metal, **reduce the spreading of the superconducting order parameter,** which leads to its greater value in the junction, and higher critical current densities. Since magnetron sputtering or electron beam evaporation are used to deposit films, the resulting metal is considered diffuse, or dirty, and the Usadel equation is used to describe superconductivity. Also, the stated conditions of the problem, namely, $d \ll \xi_N$, $S \ll \xi_N$, $w \approx \xi_N$, allow us to consider the problem to be 1-dimensional, and after some simplifications, one-dimensional. The behavior of the system depends on the parameter $\gamma_{BM} = \gamma_B \frac{d_n}{\xi_N^*} = \frac{R_B}{\rho_n \xi_N^*} \frac{d_n}{\xi_N^*}$. Current-phase relations were obtained within large and small γ_{BM}:

Small γ_{BM}:

$$\frac{eR_n J_s}{2\pi T_c} = \frac{T}{T_c} \sum_{\omega>0} \frac{\Delta \cos\frac{\phi}{2}}{\Omega_1} \arctan \frac{\Delta \sin\frac{\phi}{2}}{\Omega_1} \tag{2.21}$$

Where $\Omega_1 = \sqrt{\Omega^2 + \Delta^2 \cos^2\frac{\phi}{2}}$, $\Omega = \omega\left(1 + \gamma_{BM}\sqrt{\omega^2 + \Delta^2}\right)$, ω and Δ - Matsubara frequency and superconducting order parameter normalized to πT_c

Large γ_{BM}:

$$\frac{eR_n J_s}{2\pi T_c} = \frac{T}{T_c} \sum_{\omega>0} \frac{\sqrt{2}\Delta^2 \sin\phi}{\Omega_1 \sqrt{\left(\sqrt{\Omega^2 + \Delta^2} + \Omega_1\right)\sqrt{\omega^2 + \Delta^2}}} \tag{2.22}$$

$R_n = 2R_{sn} + R_{nb}$ - normal resistance, determined by the sum of the bridge resistance and the normal metal-superconductor boundary resistances. In the case of small γ_{BM}, the bridge resistance prevails, in the case of large γ_{BM} resistance of the boundaries prevails. Current-phase relations for different γ_{BM} and normalized temperatures shown on fig. 2.3. For temperatures close to critical temperature, or for large γ_{BM} dependence became sin-like. In other limit of low temperatures and low interface resistance dependence became saw-toothedю

The plotted dependence of the critical current on temperature for various γ_{BM} are shown

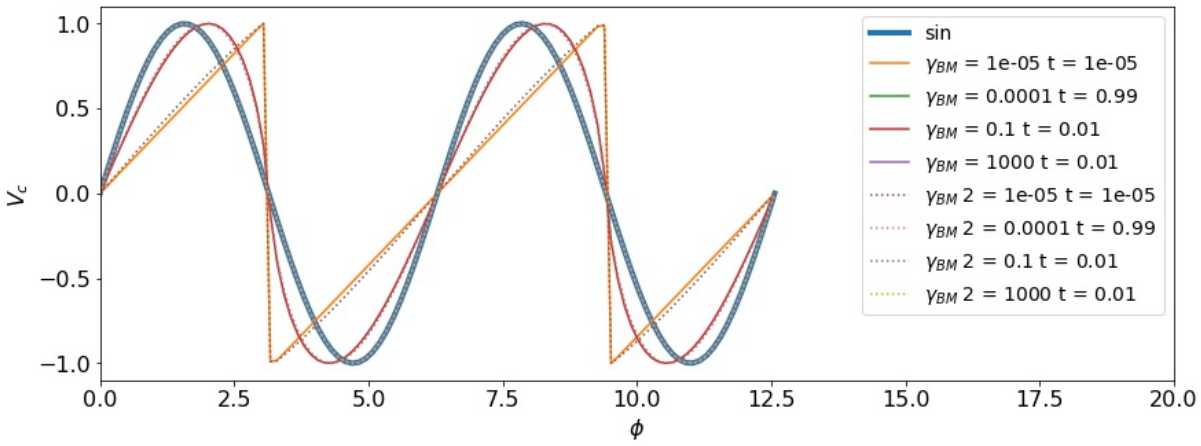

Figure 2.3: Current-phase dependence for different parameters $gamma_{BM}$ and t

in Fig. 2.4

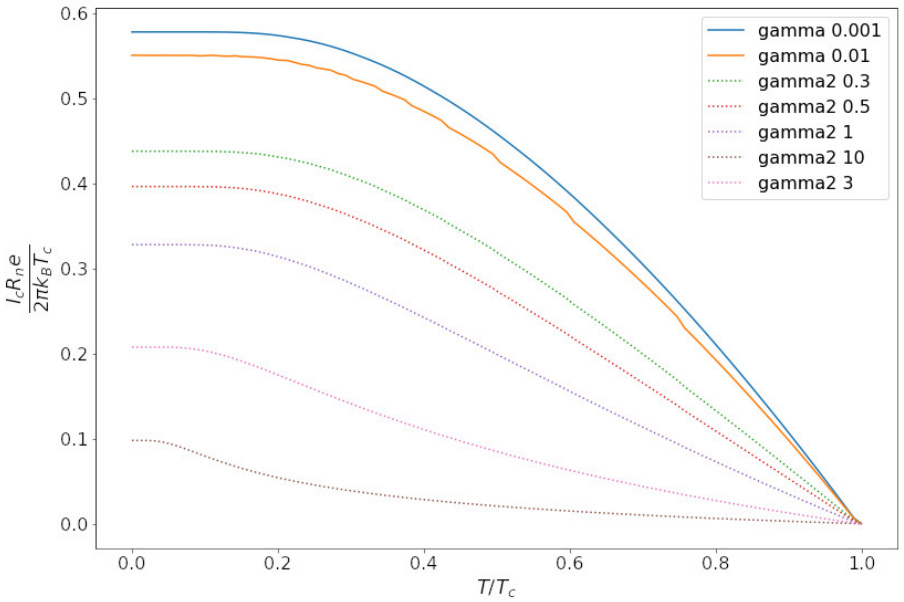

Figure 2.4: Dependence of characteristic voltage on temperature. Straight line corresponds to dependence at small gamma by formula 2.21, dotted corresponds to formula 2.22

Chapter 3

Equipment

3.1 E-beam evaporation

E-beam evaporation Utilizes Electron beam to vaporize material. [23] Firstly, free electrons emitted by thermionic source or by ionizing gaseous atoms, which acts as cathode. Crucible with evaporated material acts as anode. In order to provide passage of electrons, pressure in chamber should be less than $10^{-5}\ mbar$. Also, collisions between electrons and vaporized material should be minimized. That's why the filament is kept out of evaporation direction. Electric field $\vec{E}$ and magnetic field $\vec{B}$ can be used to increase energy of electrons and bend the beam to focus electrons to anode. Typical voltages are in range $10 - 40\ kV$ So, incoming electrons cause back scattered electrons, secondary electrons, X-rays radiation, and the greatest amount of kinetic energy converts to heat. Finally, heated and melted material produces vapour, which flows to substrate. One of the key feature of e-beam evaporation is possibility to provide anisotropic deposition, which can be used for shadow evaporation technique.

At this work Plassys MEB 550S placed in MIPT and the same machine in ISSP were used3.1.

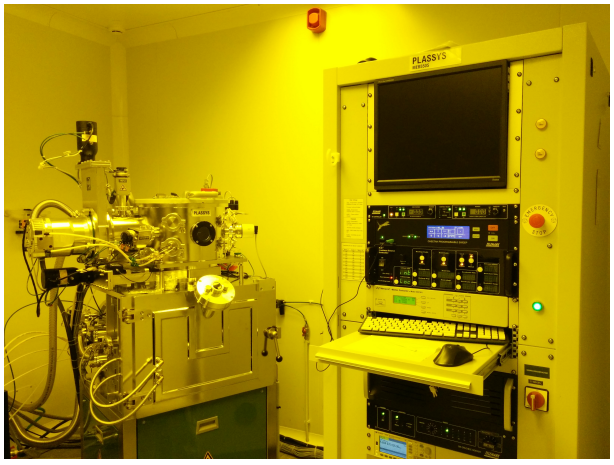

Figure 3.1: Plassys MEB 550S placed in MIPT

3.2 Ellipsometry

Ellipsometry is a method of observation and characterisation of polarised light, passing trough or reflected from interface, bi-layer or multi-layer placed in medium. This non-perturbing and sensitive tool allows to describe semi-transparent tin films in terms of film-thicknesses, complex-value refractive index and adsorption.[24]

Well known Maxwell's equations, derived in the medium allow existence of solution in the form of propagating plane electromagnetic waves. It is also called a light. In uniform medium light has two polarisations, with perpendicular directions of electric field. Propagation though the medium occurs with different speed, depending on refracting index n, which can be rewritten in therms of permittivity ϵ and permeability μ.

When polarised wave falls on the interface, two polarisations are distinguished: for s-wave electric field vector perpendicular to incident plane and for p-wave electric field vector in incident plane. If they have equal phases, they form plane polarisation. In case of phase difference $\pi/2$ circular polarisation is formed. Other cases considered as elliptical polarisation.

Ellipsometry operates with light, reflected from multi-layer. Firstly we introduce reflection coefficients for s and p waves

$$r_{p,s} = \frac{E_{r(p,s)}}{E_{i(p,s)}} \tag{3.1}$$

We can introduce ratio between complex amplitudes r_p and r_s:

$$\rho = \frac{r_p}{r_s} = \tan\Psi \exp i\Delta \tag{3.2}$$

$tan\Psi$ represents ratio between amplitudes of two perpendicular polarisation, Δ represents phase difference between two reflected waves. Ellipsometer, according to his name, measures ellipse characteristics, Ψ and Δ. Knowing thicknesses, angle of incidence, wave-length and refracting indexes of all layers, Ψ and Δ can be calculated. If we change length of light, coefficient will change, not only because of geometry, but refractive index is dependent on wave-length. There are a lot of theories to take into account this dependence, which works in different limits and different materials. for our purposes Cauchy theory is enough. [25] It takes into account even decrease of wave-length and can be applied at optical diapason.

$$n(\lambda) = n_0 + \frac{n_1}{\lambda^2} + \frac{n_2}{\lambda^4} \tag{3.3}$$

So, we suppose, there is multiplayer with certain layers with known refractive index Cauchy coefficients and we want to determine thicknesses of each layer. We though light at some angle

and measure Ψ and Δ for optical spectrum. Obtained data should be fitted this thicknesses.

In this work Ellipsometer SENTECH SER 800 placed in MIPT 3.2 was used to determine the thickness of electron resist.

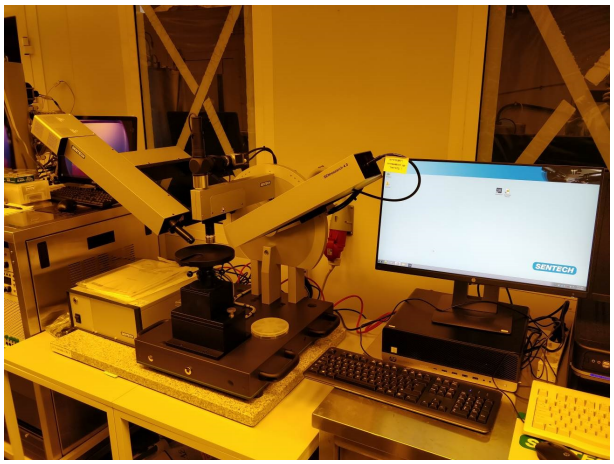

Figure 3.2: Ellipsometer SENTECH SER 800 placed in the center of collective usage, MIPT

3.3 Bluefors

BlueFors is a delusion refrigerator which can cool down down to 10 mK3.3. It has several systems for cooling. Standard for cryogenic equipment two-step Pulse Tube, which perform cooling from room temperatures to 50K and to 4K. Then, using Joule-Thomson process system coolies down to 1K. Also it used to condensate mixture of He-3 and He-4. Then evaporation of He-3 perform additional cooling to 600 mK. And the final part is cooling due to mixing of He isotopes. It allows to achieve 10 mK.

3.3.1 Delusion refrigerator

Dilution refrigerator is the system, which provide cooling down to $10\ mK$. Its principles based on He4/He3 phase diagram. [26] At temperatures above $2.17\ K$ He-4 and He-3 are in normal state.3.4 Below this temperature mixture can become superfluid, depending on He-3 concentration. At temperatures below $800\ mK$ mixture separates into two phases: He-3 rich normal state and He-3 poor super-fluid state. Near absolute zero He-3 rich phase becomes He-3 pure state. The enthalpy of He-3 rich state larger than poor state. So, when He-3 takes energy from environment when is moved from rich to poor phase, and that is how cooling occurs.

Scheme is shown on figure 3.4. He-3 flow from condensed line to Still pumping line is organized to provide heat flow from He-3 rich phase to poor phase. The He-3 pumped from still carry away heat and free the space for new He-3. Incoming He-3 to mixing chamber take a heat when move to He-3 poor state.

Figure 3.3: Side view of BlueFors

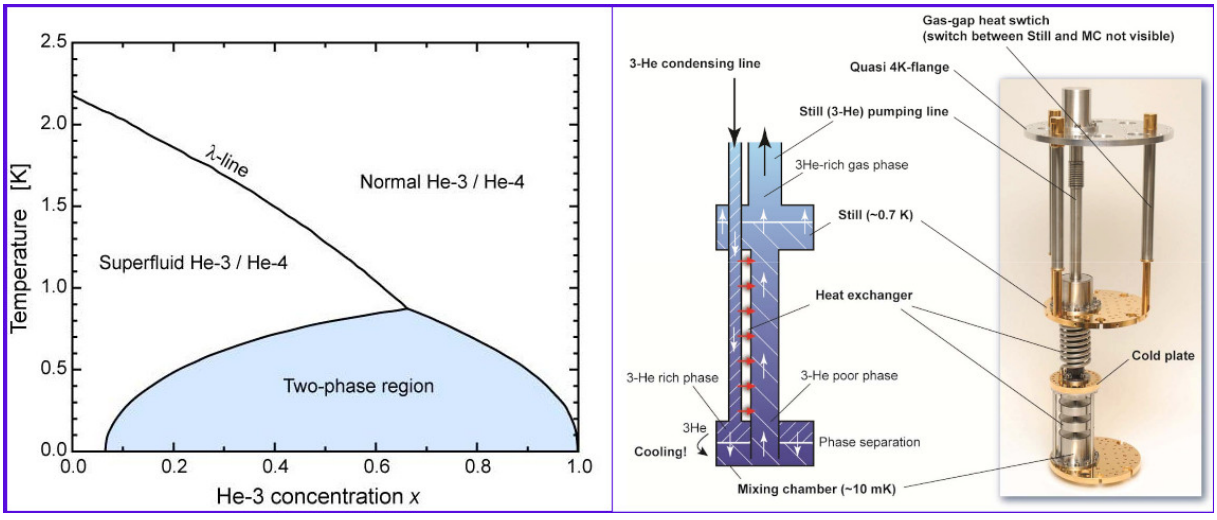

Figure 3.4: **Left**. Phase diagram of He-3/He-4 mixture. **Right**. Scheme of mixing chamber

Chapter 4

Results and discussion

4.1 Sample fabrication

For sample fabrication we have tried different methods, etching though aluminum mask, etching through resist mask, two step etching, and shadow evaporation trough two-layer resist mask. It happened the last one appeared most successful, and at this part fabrication via shadow evaporation technique is described.

4.1.1 Design

Based on the theory, where JJ with the gap of size less then ξ_N was described, Electron lithography was used to achieve required accuracy. Two step lithography was chosen. At the first design step there is a large massive of JJ with wide range of gap sizes and overlaps. It was done to overcome differences between design and final object. During lithography, development step, errors can be accumulated. But If the is a lot of different structures, only successful ones can be chosen. At the second step we can connect them with incoming contacts. The whole process has shown on the figure 4.1.

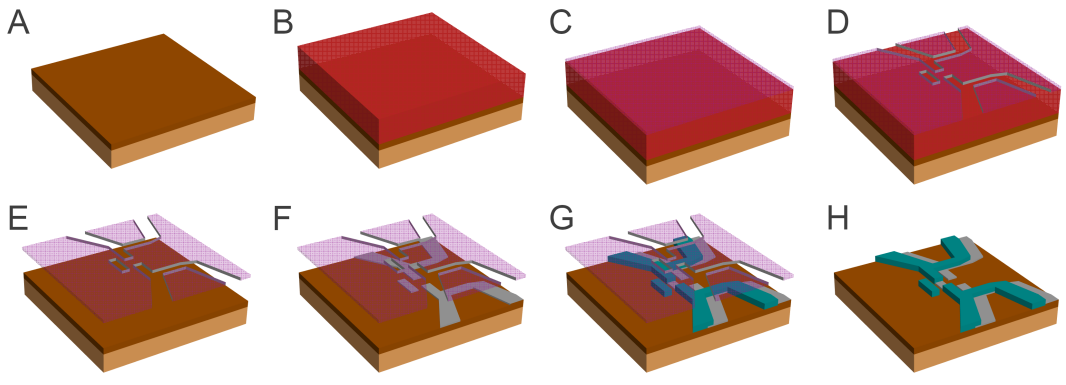

Figure 4.1: Full fabrication process of planar SNS. **A**. Stand alone silicon oxidised substrate. **B**. Deposition of approximately 760 m of MMA resist using spin-coating technique. **C**. Spin-coating deposition of ARP-6200.04 electron resist. **D**. Electron lithography and upper resist layer development. **E**. Co-polymer layer development. Caves formation **F**. Aluminum layer deposition. **G**. Niobium layer deposition. **H**. Lift-off process.

4.1.2 Lithography

Zelenograd production silicon (100) substrate, doped with boron, and with $270\ nm$ of Oxide was chosen for samples, while for dc measurements at low temperatures type of substrate no so important.

For shadow evaporation two layer resist is used. The first buffer layer is optical resist MMA. Parameters are shown in the list below:

- Substrate ultrasound cleaning at acetone, IPA, H_2O, O_2 plasma cleaning
- **MMA** Co-polymer resist (2 layers)
  - Heating before cleaning at 160°C
  - Depositing resist on substrate using spin-coating technique with rotation speed **3000 rpm** during **1 minute**. (each layer)
  - baking at temperature 160°C during 5 min (each layer)
  - Final thickness is about $760\ nm$
- **ARP 6200.04** electron resist
  - Depositing resist on substrate using spin-coating technique with rotation speed **4500 rpm** during **1 minute**.
  - baking at temperature 160°C during 5 min
  - Final thickness is about $56\ nm$
- Electron lithography
  - Field size $300\mu m$
  - Resist sensitivity $160\ \mu C/cm^2$
  - Beam current $360\ pA$
  - Dose timer $1\ \mu s$ per point
- Resist development
  - Upper layer development using ARP-600-546 in 1 minute
  - IPA during 30 seconds and water in 30 s
  - Co-polymer development with $IPA + H_2O$ mixture with proportion $93\% + 7\%$ during 7 min (Fig. 4.2)

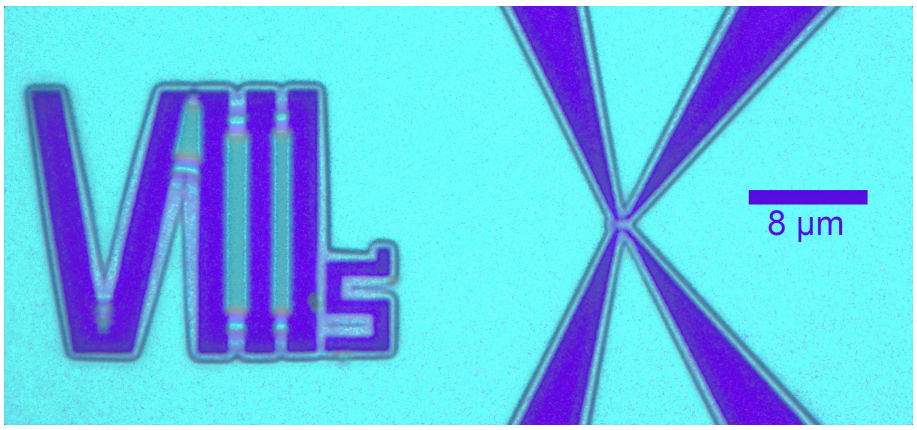

Figure 4.2: Ordinary Co-polymer development. It can be sen on the boundaries depth of cavities.The size of the roof on the contacts is 400 nm.

4.1.3 Metal deposition

Before shadow evaporation resist thicknesses were precisely determined using ellipsomery technique. It is important for deposition angles calculation. Cauchy indexes used in calculations are listed in the table 4.1. Measurements were performed on the angle 60° Obtained data and fit are shown on fig. 4.3.

Table 4.1: Fitting parameters for ellipsometry

Layer	Fitted	Thickness, nm	N0	N1, $10^2 \times nm^2$	N2, $10^7 \times nm^4$
Air	no	–			
AR-P 6200 (CSAR 62)	yes	55	1.543	71.4	0
MMA 8.5mEL (CKP)	yes	764	1.478	7.204	34.78
SiO2 (Pliskin)	no	270	1.462	36	0
Silicon (100) (Jellison)	no	–			

Determined thicknesses is

This thicknesses distinguish of table values at used spin-coating parameters. It may occur because of insufficient conditions of resist storage or just because of drying during the time.

Deposition angel was calculated using the following formula:

$$\alpha = arctan\frac{S}{H + L/2} \tag{4.1}$$

Shadow evaporation was done with two PLASSYS (fig 3.1), placed in ISSP, Chernogolovka and MIPT, Dolgoprudny. Vacuum chamber was pumped out during about 16 hours to achieve pressure near $10^{-8}\ mbar$. Before deposition samples were cleaned with plasma two times under $250\ V$ and $10\ mA$.

- **Aluminum** deposition (Fig. 4.4.a)
  - Pressure during deposition $3.5 \times 10^{-8}\ mbar$

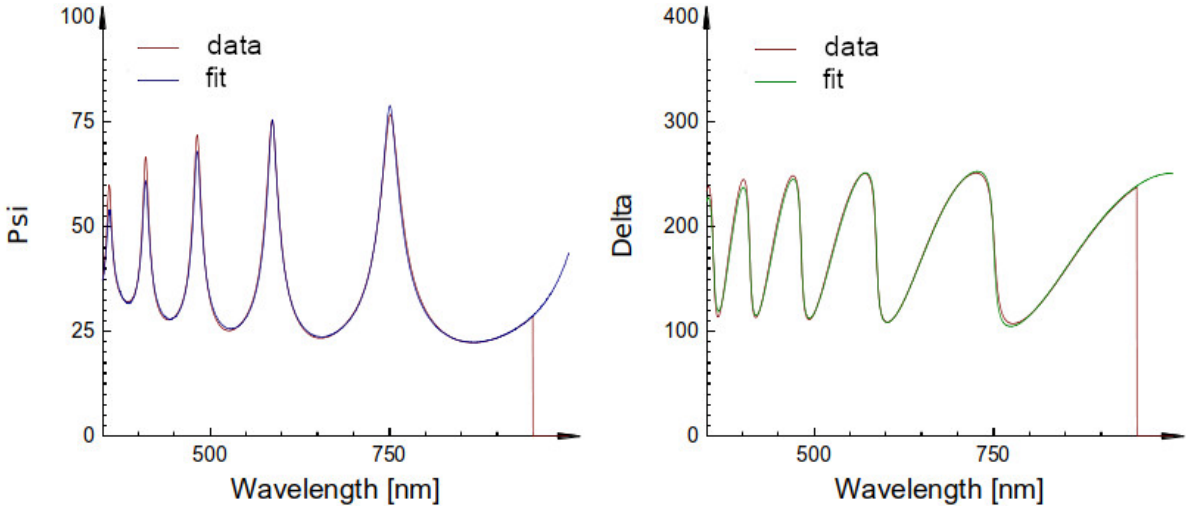

Figure 4.3: Ψ and Δ parameters measured at wave-length range from 350 nm to 950 nm, and fitting curves

  - rotation angle 16.2°
  - thickness $30nm$
  - Speed of deposition is $0.5\ nm/s$

- **Niobium** deposition (Fig. 4.4.b)
  - Pressure during deposition $1.5 \times 10^{-8}\ mbar$
  - rotation angle 0°
  - thickness $80nm$
  - Speed of deposition is $0.5\ nm/s$

When deposition has finished, we made lift-off in NMP at temperature 105°, and washed at acetone, IPA, water.

In design structures were drawn without supplying contacts, in order to save space and increase number of junctions. After Lift-Off samples were observed in SEM to choose most promising structures. With second lithography we made supplying contacts mask, and deposited **5 nm of Ti** and **45 nm of Nb**. We didn't make cleaning before second deposition, so at overlapping area we obtained large resistance. And final part is the second lift-off. SEM images of obtained JJ are shown on the fig. 4.5.

4.2 Measurements

When sample have been fabricated, it was connected to the sample holder using ultra-sonic bonding machine4.7. During connection of the micro-wires all pads a connected to each other, to avoid Then sample can be placed in refrigerator .

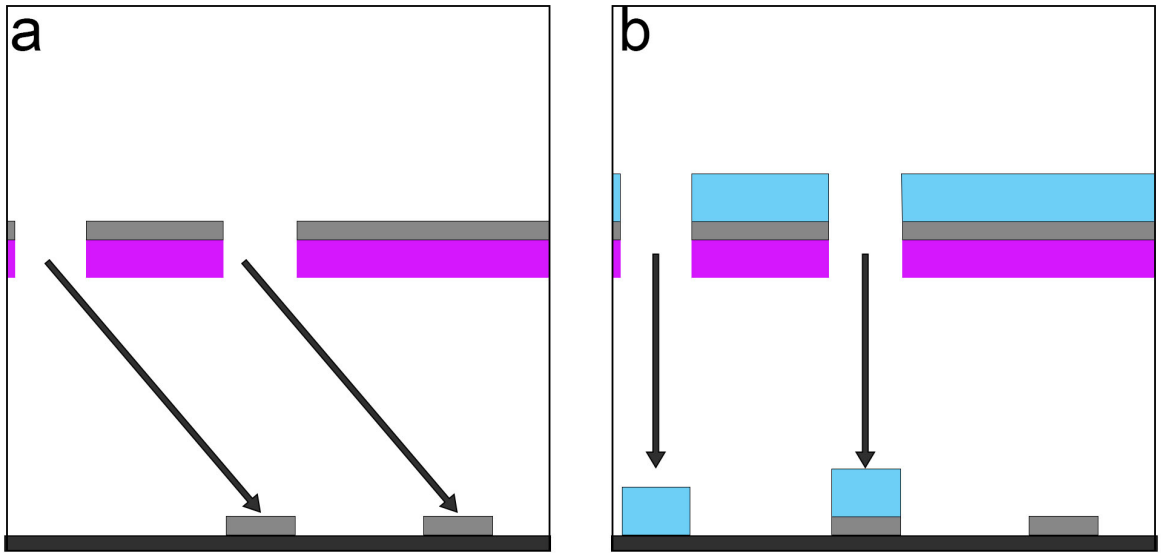

Figure 4.4: Shadow evaporation process. **a.** Al 30 nm deposition at an angle of 16.2°. **b.** Nb 80 nm deposition at right angle.

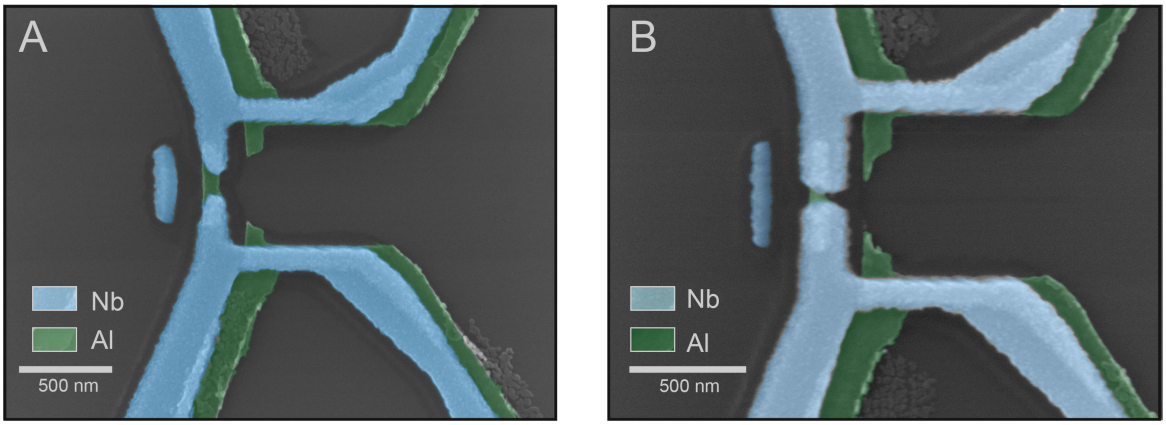

Figure 4.5: SEM image of measured Josephson contacts. A. **Sample A**. Gap size is **120 nm**, width of bridge **86 nm** B. **Sample B**. Gap size is **36 nm**, width of bridge **63 nm**

Measurements were carried out at BlueFors delusion refrigerator. 24 lines are connected to one sample holder4.7. Connection to that lines implemented using connection box. For Current-Voltage dependence measurements with 4-point probe method combination of current source **Keithley 6221** and nano-voltmeter **Keithley 2182** is used. Also each line had high frequencies RC-filters with cut-off frequency about $1\ kHz$. Them where placed at 4 Kelvin plate to avoid heating of 10 mK plate because of resistors in filters.

While we obtained large resistance in supplying contacts, not in the Josephson Junction, even at 15 mK, we had noticeable noise. That is why data was smoothed using LOWESS algorithm[27]. Example of smoothing is shown on the fig. 4.8. Current-voltage curves we in the range of temperatures from 10mK to 10K were measured

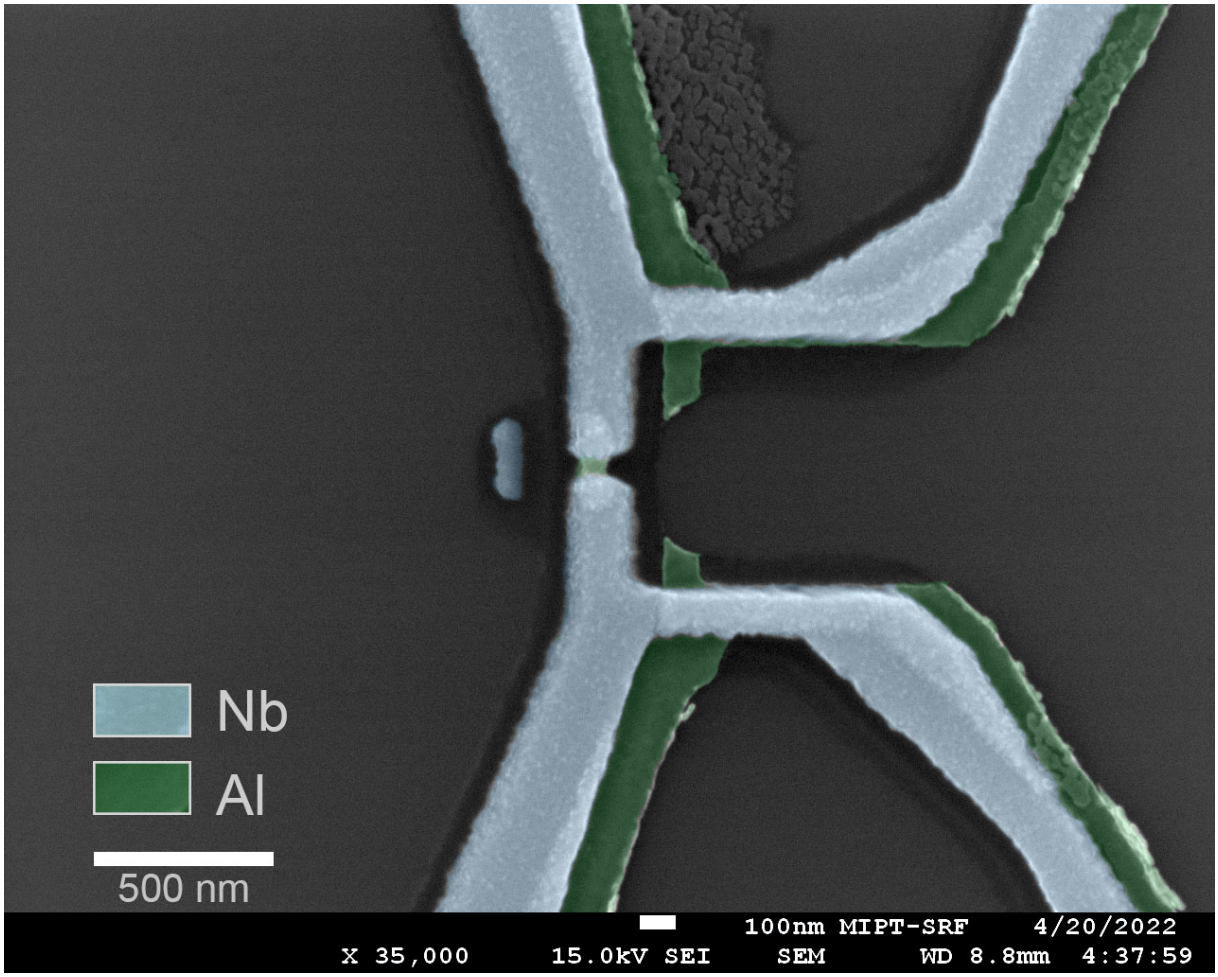

Figure 4.6: SEM image of Sample E

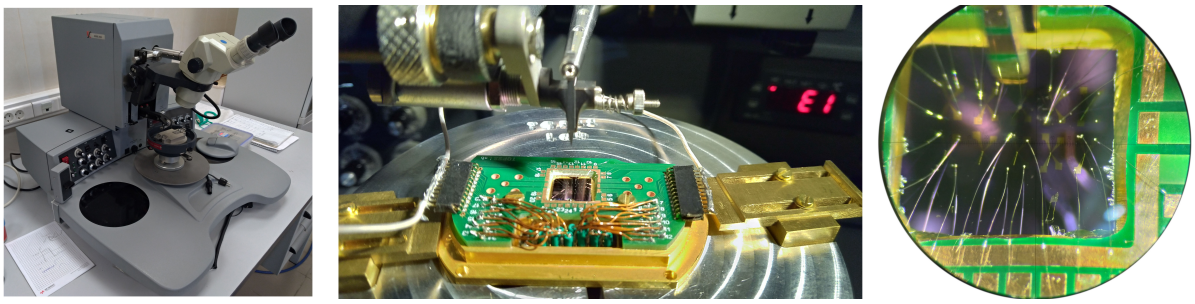

Figure 4.7: Bonding-related equipment. **Left**. Ultra-sonic micro-welding machine K&S 4526. **Center** Sample holder for low-temperature part placed on table for bonding. **Right** Samples on the silicon substrate, connected to holder via aluminum micro-wires.

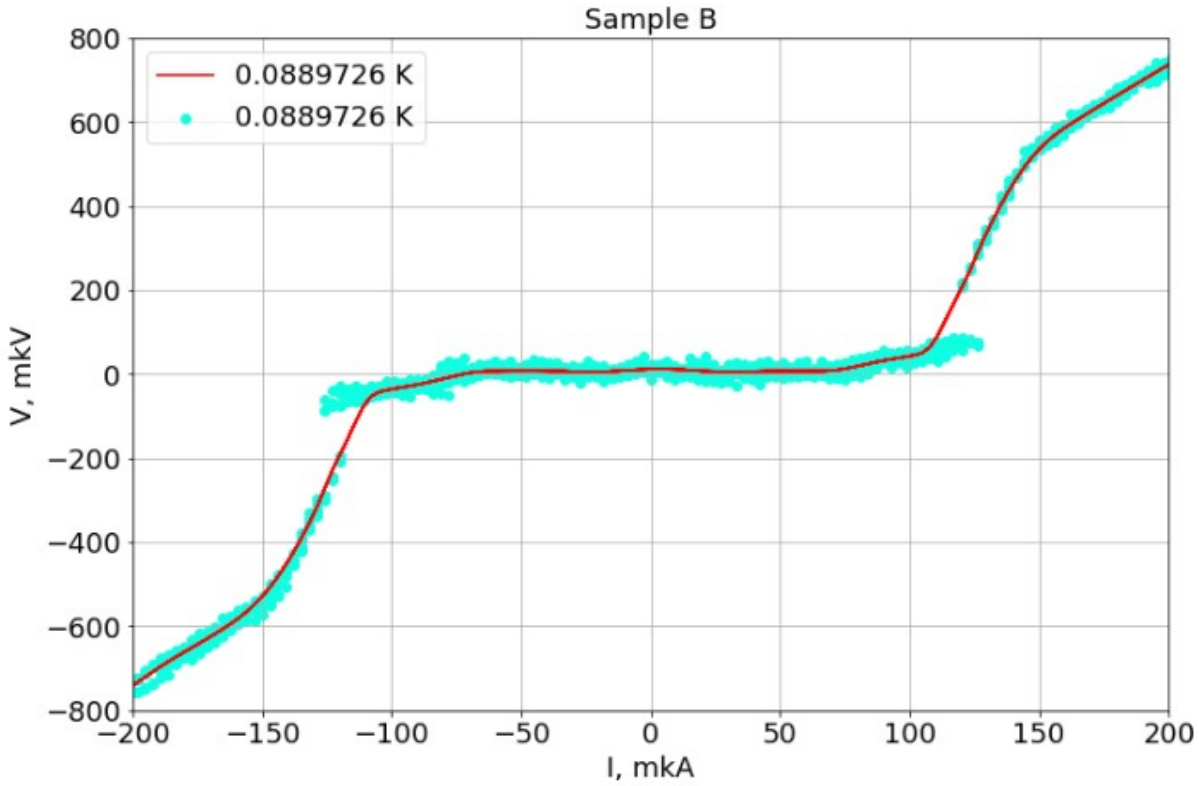

Figure 4.8: Example of LOWESS smoothing. Points represents initial data. Straight line shows the result of smoothing.

4.3 Results

Measured curves are shown on the picture 4.11. It can be seen, that curves have two bending points. They can be associated with tow geometrically distanced places, where superconductivity breaks down. The first one is the area of Al between Nb bridges. At temperatures above and below of critical temperature of aluminum, order parameter weaker then inside bridges or under them. This resistance can be estimated. Firstly, we take standard low temperature resistance of square aluminum film with thickness 20 nm, $R_{sq} = 1.5\ \Omega$, which is usually obtained with Plasyss. Then, using thickness 30 nm, width - 63 nm and length - 37 nm, calculated resistance will be $R = R_{sq}\frac{20\ nm}{30\ nm}\frac{37\ nm}{63\ nm} = 0.6\ \Omega$, which is close to the first resistance. The second bending point depict superconductivity break down under electrodes. Critical currents usually are well seen on differential resistance maps (fig. 4.9). Second critical current is well seen on the both maps, but the first can be seen for Sample B only. It is result of high noise and comparably low first resistance. So, for sample A extracted critical current are less accurate (fig. 4.11).

For the Sample E(fig. 4.6) it can be seen, that normal resistance at higher voltages equal to resistance at 12 K, in other words above critical temperature of Nb. That means superconductivity in Nb bridges is fully destroyed by current. The close positions of the first and second critical currents points on high proximity.

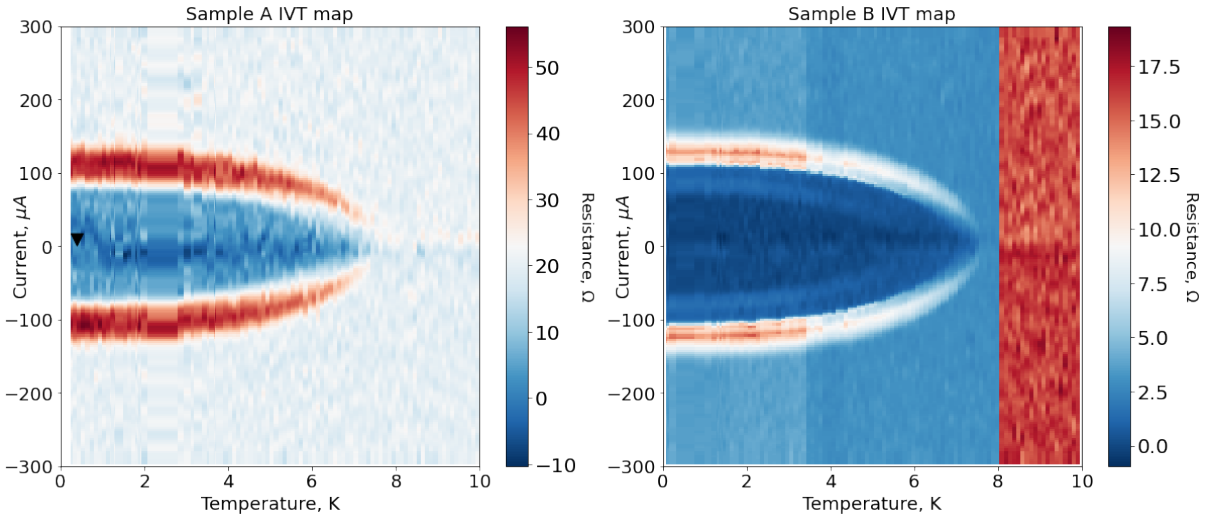

Figure 4.9: Differential resistance dependence on temperature and current for samples A and B. For the sample B steps in resistance can be seen. It looks like artefact of measurements., Because of step on 4 K in not reproducible , and $16; \Omega$ is more likely true based on RRR coefficient. The reason of such behavior be related with short-circuits of bonding wires, which bend because temperature stress.

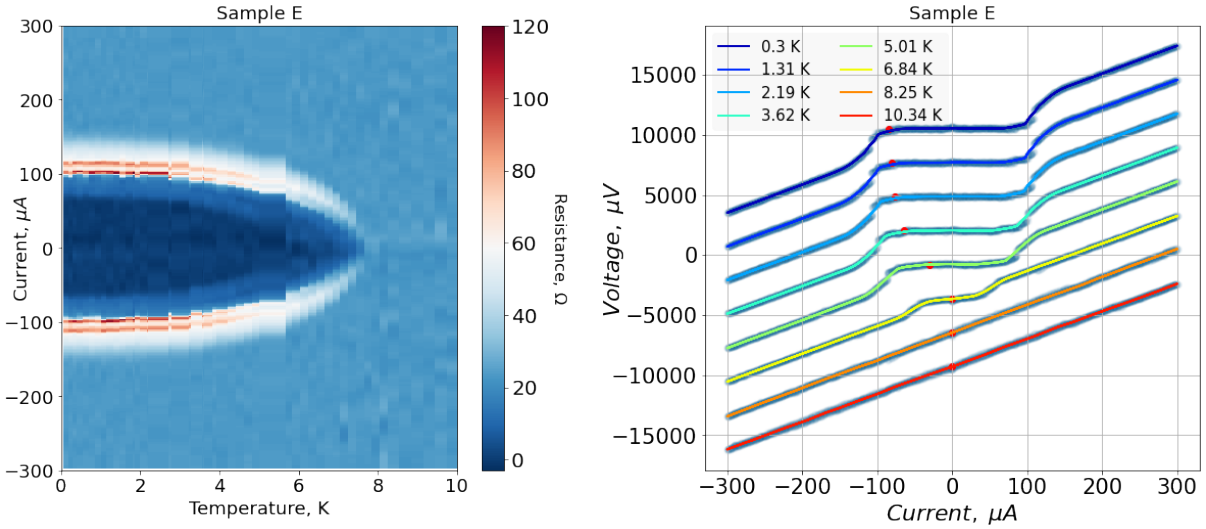

Figure 4.10: Resistance map and current voltage curves for sample E

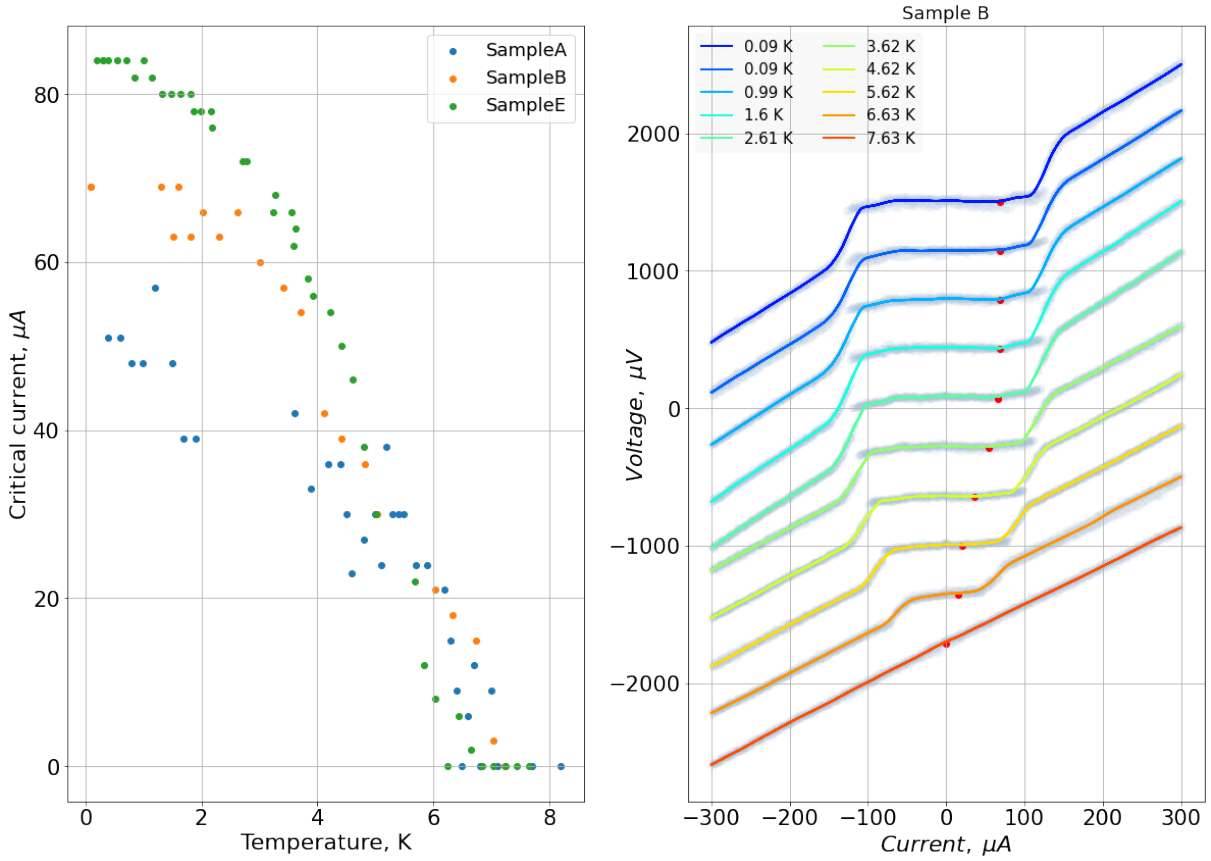

Figure 4.11: Left picture represents critical currents for different samples. Right picture shows current-voltage curves for Sample B. Blue points are represents initial data in **both** directions simultaneously . Straight lines represent smoothed data. Red points show the critical current.

Table 4.2: Normal resistance of samples

Sample	R_{low}	R_{room}	RRR	S, nm	W, nm	$j_s,\ mA/\mu m^2$ T = 0K	$j_s,\ mA/\mu m^2$ T = 4K
A	20	35	1.75	120	86	20	10
B	16 (3)	32	2 (10)	37	63	37	22
E	23	38	1.65	50	70	39	26

Residual-resistance ratio (RRR) for samples is on the order of 1.7 (Tab. 4.2). For highly pure Nb this ratio may achieve values of 300, good ratio can be between 5-10, our Nb is far from purity. One of explanations is bad interface between Al and Nb, which can be a consequence of chosen electron beam evaporation technique.

Obtained critical current dependencies can be fitted with the theory of short VTB.

And the last, but not the least is the main fact, why such junctions were studied. All samples are hysteresis free 4.11, even at very low temperatures of order $10\ mK$. This coincides with high critical current densities (Tab. 4.2), all of them higher then

4.4 Conclusions

In conclusion, short and long planar Josephson junctions, in variable-thickness bridge geometry were fabricated and studied. During the work main and side tasks were resolved. Major outcomes, which should be emphasised are:

- It was shown, that short planar Josephson junctions can be hysteresis free. While Nb and Al combination is commonly used in superconducting computing, such junctions can be easily integrated to existing technical processes. So, opportunity to increase the density of elements by order appears possible.
- Adjustment for such technology is needed. Rate of successfully produced junctions with usage of electron lithograph was on the order of 60%. Of course only few iterations were done during the work, the question of reproductivity is important. At large circuits thousands of elements must be successfully produced at ones. But, in this work only potential variable-bridge approach was shown.
- Studied samples show characteristic voltages on the order higher in comparison with currently used in superconducting electronics tunnel barriers. It influences on duration of duration of switching current pulses, which means operating frequenters can be increased in case of planar weak link implementation.
- Theory of short VTB was checked on real samples. While the article is relatevly new, experimental verification was required.

So, this work has shown potential advantages of VTB over shunted SIS junctions. Future work can be concentrated on improvement of technology and application to an simple arithmetical circuits.

4.5 Appendix: Issues overview

This part contain information about consequences of wrong decisions during samples fabrication.

4.5.1 Mismatching of two layers

During resist deposition using spin-coating, extra resist is though away because of centrifugal force. Thickness of resist depend on combination of time and rotation speed. But thickness is not uniform all over the substrate. Besides local roughness, thickness of resit higher close to edges of substrate. This difference not so large, but it's enough to broke matching during shadow evaporation.4.12

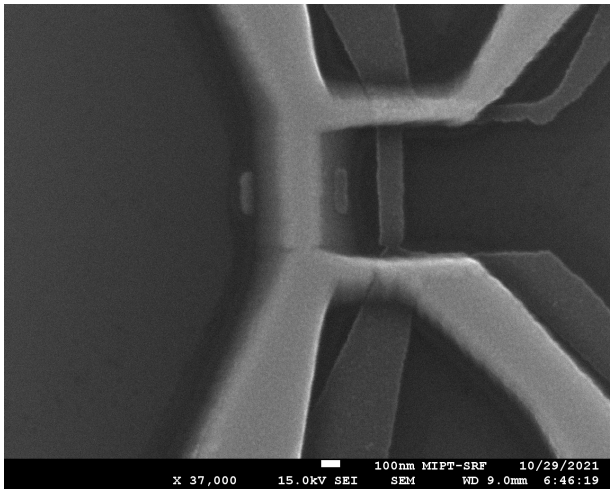

Figure 4.12: Layers mismatching because of higher thicknesses on the edges of substrate

4.5.2 poor vacuum

It is necessary to have deep vacuum during metal evaporation. Electron beam evaporation can operate from pressures near $10^{-5}\ mbar$. Even at pressure range $10^{-7} - 10^{-6}\ mbar$ superconducting Nb with critical temperature $T_{Nb} = 8.5\ K$ and Al with critical temperature $T_{Al} = 1.5\ K$ can be obtained. Samples produced at such conditions have shown superconductivity, but only at temperatures less then T_{Al}. When one of samples was measured with 3-point probe method, superconducting step of Nb on resistance dependence on temperature was observed(fig. 4.13), so Nb still superconducting. But, measurements of samples with 4-point probe don't show superconductivity at temperatures above T_{Al}. That fact are evidences of large resistance of interface between Nb and Al. In other words proximity don't occur thought the boundary. Another sign is resistance dependence on the temperature. Resistance decreasing with increasing of the temperature. This behavior is non-metalik and looks like semiconductor behavior.

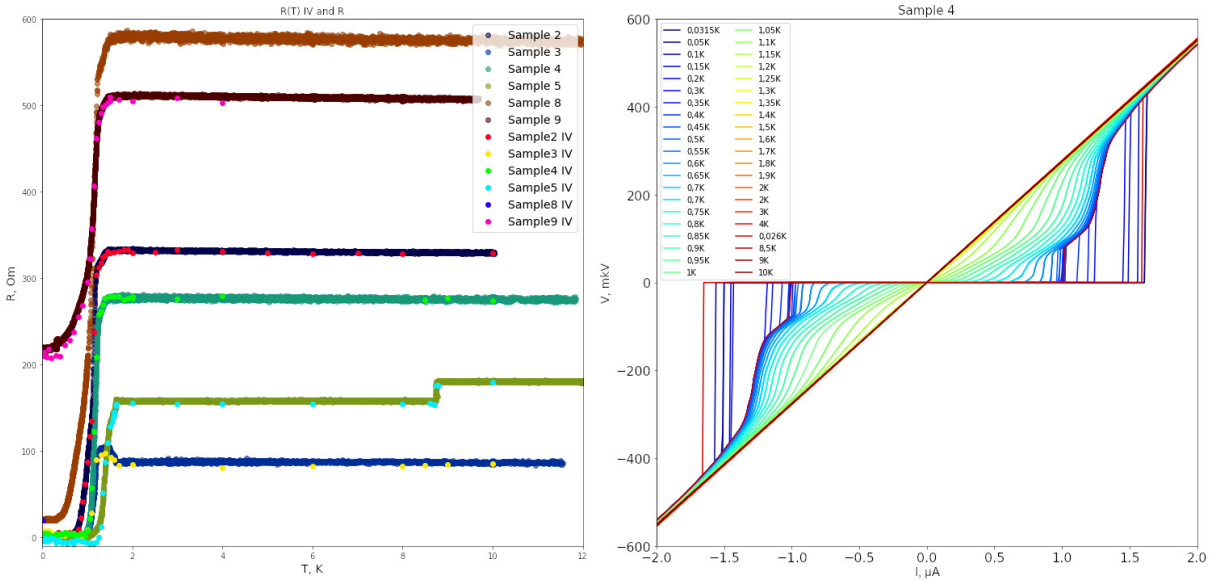

Figure 4.13: Resistance dependence on temperature and Current voltage relation for on of the sample in series

4.5.3 design shift

Some times final sample can be ruined because of lithography process(fig. 4.14). Program bugs can shift parts of design on several nanometers. This accrues on the stretching between to nearest fields.

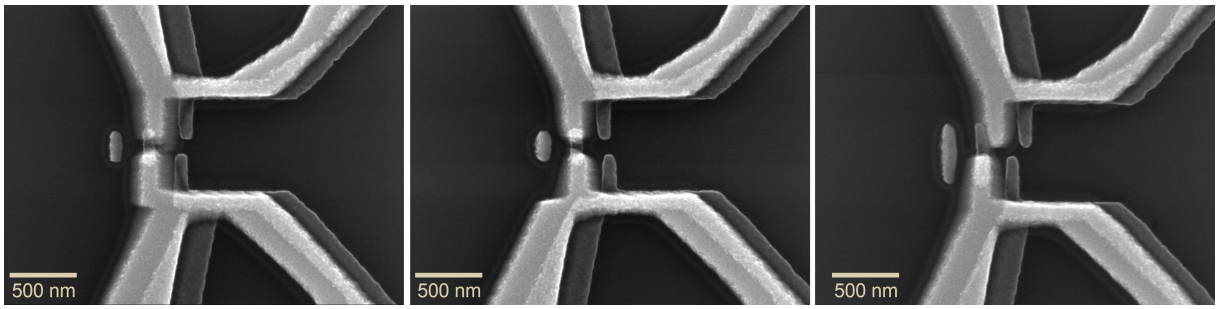

Figure 4.14: Misalignment of neighbour fields during lithography process

Bibliography

[1] S. K. Tolpygo, "Superconductor digital electronics: Scalability and energy efficiency issues (review article)," *Low Temperature Physics*, vol. 42, no. 5, pp. 361–379, 2016. [Online]. Available: https://doi.org/10.1063/1.4948618

[2] V. V. Schmidt, P. Müller, and A. V. Ustinov, *The Physics of Superconductors*, 1997. [Online]. Available: https://doi.org/10.1007/978-3-662-03501-6

[3] B. Josephson, "Possible new effects in superconductive tunnelling," *Physics Letters*, vol. 1, no. 7, pp. 251–253, 1962. [Online]. Available: https://www.sciencedirect.com/science/article/pii/0031916362913690

[4] K. Likharev and V. Semenov, "Rsfq logic/memory family: a new josephson-junction technology for sub-terahertz-clock-frequency digital systems," *IEEE Transactions on Applied Superconductivity*, vol. 1, no. 1, pp. 3–28, 1991. [Online]. Available: https://doi.org/10.1109/77.80745

[5] K. K. Likharev, "Superconducting weak links," *Rev. Mod. Phys.*, vol. 51, pp. 101–159, Jan 1979. [Online]. Available: https://link.aps.org/doi/10.1103/RevModPhys.51.101

[6] A. A. Golubov, M. Y. Kupriyanov, and E. Il'ichev, "The current-phase relation in josephson junctions," *Rev. Mod. Phys.*, vol. 76, pp. 411–469, Apr 2004. [Online]. Available: https://link.aps.org/doi/10.1103/RevModPhys.76.411

[7] J. Bardeen and J. L. Johnson, "Josephson current flow in pure superconducting-normal-superconducting junctions," *Phys. Rev. B*, vol. 5, pp. 72–78, Jan 1972. [Online]. Available: https://link.aps.org/doi/10.1103/PhysRevB.5.72

[8] D. E. McCumber, "Effect of ac impedance on dc voltage-current characteristics of superconductor weak-link junctions," *Journal of Applied Physics*, vol. 39, no. 7, pp. 3113–3118, 1968. [Online]. Available: https://doi.org/10.1063/1.1656743

[9] T. A. Fulton and L. N. Dunkleberger, "Origin of hysteresis in the i□v curves of point□contact junctions," *Journal of Applied Physics*, vol. 45, no. 5, pp. 2283–2285, 1974. [Online]. Available: https://doi.org/10.1063/1.1663577

[10] A. Rogachev, A. T. Bollinger, and A. Bezryadin, “Influence of high magnetic fields on the superconducting transition of one-dimensional nb and moge nanowires,” *Phys. Rev. Lett.*, vol. 94, p. 017004, Jan 2005. [Online]. Available: https://link.aps.org/doi/10.1103/PhysRevLett.94.017004

[11] L. Angers, F. Chiodi, G. Montambaux, M. Ferrier, S. Guéron, H. Bouchiat, and J. C. Cuevas, “Proximity dc squids in the long-junction limit,” *Phys. Rev. B*, vol. 77, p. 165408, Apr 2008. [Online]. Available: https://link.aps.org/doi/10.1103/PhysRevB.77.165408

[12] Y. Song, “Origin of ”capacitance” in superconducting microbridges,” *Journal of Applied Physics*, vol. 47, no. 6, pp. 2651–2655, 1976. [Online]. Available: https://doi.org/10.1063/1.322985

[13] H. Courtois, M. Meschke, J. T. Peltonen, and J. P. Pekola, “Origin of hysteresis in a proximity josephson junction,” *Phys. Rev. Lett.*, vol. 101, p. 067002, Aug 2008. [Online]. Available: https://link.aps.org/doi/10.1103/PhysRevLett.101.067002

[14] W. Anacker, “Josephson computer technology: An ibm research project,” *IBM Journal of Research and Development*, vol. 24, no. 2, pp. 107–112, 1980. [Online]. Available: https://doi.org/10.1147/rd.242.0107

[15] R. E. Miller, W. H. Mallison, A. W. Kleinsasser, K. A. Delin, and E. M. Macedo, “Niobium trilayer josephson tunnel junctions with ultrahigh critical current densities,” *Applied Physics Letters*, vol. 63, no. 10, pp. 1423–1425, 1993. [Online]. Available: https://doi.org/10.1063/1.109697

[16] S. K. Tolpygo, V. Bolkhovsky, S. Zarr, T. J. Weir, A. Wynn, A. L. Day, L. M. Johnson, and M. A. Gouker, “Properties of unshunted and resistively shunted nb/alox-al/nb josephson junctions with critical current densities from 0.1 to 1 ma/μm2,” *IEEE Transactions on Applied Superconductivity*, vol. 27, no. 4, pp. 1–15, 2017. [Online]. Available: https://doi.org/10.1109/TASC.2017.2667403

[17] I. Soloviev, S. Bakurskiy, V. Ruzhickiy, N. Klenov, M. Kupriyanov, A. Golubov, O. Skryabina, and V. Stolyarov, “Miniaturization of josephson junctions for digital superconducting circuits,” *Phys. Rev. Applied*, vol. 16, p. 044060, Oct 2021. [Online]. Available: https://link.aps.org/doi/10.1103/PhysRevApplied.16.044060

[18] Y. P. Baryshev, A. Vasil’ev, A. Dmitriyev, M. Y. Kupriyanov, V. Lukichev, I. Y. Luk’yanova, A. Orlikovskiy, and I. Sokolova, “Theoretical and experimental study of the josephson effect in submicron sn-n-ns structures,” *Lithography in microelectronics*, vol. 8, p. 187, 1989.

[19] P. Dubos, H. Courtois, B. Pannetier, F. K. Wilhelm, A. D. Zaikin, and G. Schön, “Josephson critical current in a long mesoscopic s-n-s junction,” *Phys. Rev. B*, vol. 63, p. 064502, Jan 2001. [Online]. Available: https://link.aps.org/doi/10.1103/PhysRevB.63.064502

[20] C. P. GarcΓa and F. Giazotto, “Josephson current in nanofabricated v/cu/v mesoscopic junctions,” *Applied Physics Letters*, vol. 94, no. 13, p. 132508, 2009. [Online]. Available: https://doi.org/10.1063/1.3114522

[21] T. E. Golikova, F. HΓjbler, D. Beckmann, N. V. Klenov, S. V. Bakurskiy, M. Y. Kupriyanov, I. E. Batov, and V. V. Ryazanov, “Critical current in planar sns josephson junctions,” *JETP Letters*, vol. 96, no. 10, pp. 668–673, 2013. [Online]. Available: https://doi.org/10.1134/S0021364012220043

[22] R. H. Ono, J. E. Sauvageau, A. K. Jain, D. B. Schwartz, K. T. Springer, and J. E. Lukens, “Suspended metal mask techniques in josephson junction fabrication,” *Journal of Vacuum Science & Technology B: Microelectronics Processing and Phenomena*, vol. 3, no. 1, pp. 282–285, 1985. [Online]. Available: https://doi.org/10.1116/1.583246

[23] K. S. Harsha, *Principles of Vapor Deposition of Thin Films*, 2006. [Online]. Available: https://doi.org/10.1016/B978-0-08-044699-8.X5000-1

[24] R. Azzam, N. Bashara, and N. Bashara, *Ellipsometry and Polarized Light*, ser. Ballard CREOL collection. North-Holland Publishing Company, 1977. [Online]. Available: https://books.google.ru/books?id=1_4uAQAAIAAJ

[25] U. Richter, G. Dittmar, and H. Ketelsen, *SpectraRay/4 manual*, Sentech Instruments GmbH, 2017.

[26] *BF-LD250 User Manual*, BlueFors Cryogenics.

[27] W. S. Cleveland, “Robust locally weighted regression and smoothing scatterplots,” *Journal of the American Statistical Association*, vol. 74, no. 368, pp. 829–836, 1979. [Online]. Available: https://www.tandfonline.com/doi/abs/10.1080/01621459.1979.10481038